20 phase steps were used in the measurement. That is, the ruling is displaced in T/20 intervals, which with the specified period comes to 10μm. It is stated that the weighted sums for C(x,y) and S(x,y) in synchronous phase detection techniques compensate for the non-sinusoidal shape of the intensity variation, so phase calculations equivalent to those of interferometry may be performed. The experimental setup is shown in Fig.5.2.6.

Fig.5.2.6: Experimental setup used in [Yatagai 1984] and [Omura 1988]

The same work is continued in [Omura 1988], where detailed expressions for the phase analysis of the ronchigram are presented. Based on the same diffractive approach of the Ronchi test that was described in Section 3.1 of this work, a wave theory of the Ronchi test is developed in order to obtain phase measurements. In order to retrieve the wavefront phase, the C(x,y) and S(x,y) measured values are related to the wavefront phase following the Taylor series

$$\Phi(x,y) = \operatorname{atan}\left(\frac{S(x,y)}{C(x,y)}\right) \approx \frac{2\pi}{\lambda}\left\{ s\frac{\partial\omega(x,y)}{\partial x} + \frac{s^3}{3!}\frac{\partial^3\omega(x,y)}{\partial x^3} + \ldots \right\} \qquad (5.2.19)$$

where s is the shear of the wavefront introduced by the Ronchi test and $\omega(x,y)$ is the wavefront shape. Terms of orders higher than $\frac{\partial\omega(x,y)}{\partial x}$ are considered negligible, so the first derivative of the wavefront shape may then be measured and integrated following a least-squares method. In the experimental setup a 0.2mm period ruling is used, and 100 image frames are added up in order to reduce the statistical noise at

each step. The technique is applied to a 36.25mm diameter, 125.0mm focal length spherical lens, yielding a reported height measured range of 50μm, which may be varied by changing the period of the ruling. In this paper only 10 ruling displacements are used in order to provide phase shifts (with the ruling used, these displacements amount to 20μm each). The estimated phase measurement error, compared with a polynomial interpolation, comes to 0.39rad rms. In profile height measurements, this error is equal to 1.7μm rms for a maximum height below 50μm.

[Wan 1990] proposes an alternative scheme in order to perform phase measurements using the Ronchi test technique. Quick and simple phase measurements are said to be obtained if phase is considered a quantity proportional to the intensity of the ronchigram. The error incorporated by this linear approximation to a sinusoidal intensity profile can be reduced by averaging many interferograms with random initial phase. Two of these multiple averaged ronchigrams, with a $\pi/2$ phase shift between them, are then averaged again in order to remove most of the error introduced by the direct relation between phase and intensity. The obtained intensity is then normalized. In order to obtain fringe patterns with good fringe visibility, the system is illuminated with a tungsten lamp source converging on a small spot on the Ronchi ruling (Fig.5.2.7), which becomes a non-coherent extended source with its spatial coherence function $\xi(x)$ given by the Van Cittert-Zernicke theorem, expressed in this case as

$$\xi(x) = \mathrm{rect}\left(\frac{x}{a}\right) \cdot \mathrm{comb}\left(\frac{x}{T}\right) \otimes \mathrm{rect}\left(\frac{x}{0.5T}\right) \qquad (5.2.20)$$

where *a* is the extension of the illuminated area along the X axis, T is the period of the ruling and $\otimes$ stands for convolution. By varying the *a* distance the coherence function of the source may be modified, yielding only interference between the non-diffracted order and the plus and minus first orders. The diffractive high order terms are thus eliminated through the variation of the degree of coherence of the source.

The technique was then applied to measuring a surface profile of an aspherical parabolic mirror with 54mm diameter and 97mm focal length, and to a spherical surface of 42mm diameter and 418.2mm radius of curvature. Rulings with a 0.254mm period are used for the aspherical mirror and with a 0.127mm period for the spherical surface, showing the ability of the technique to deal with both great and small amounts of aberration. In order to measure phase along the X and Y directions of the surface, ronchigrams must be registered at orthogonal positions of the grating. Accuracy is

claimed to be better than $\pm\frac{T}{30}$. As experiments were made with a 100lpi ruling, the precision claimed for the system is 8.5μm.

Fig.5.2.7.- Experimental setup for [Wan 1990] and [Wan 1993]

The same principle is followed in [Wan 1993] in order to study to what extent the period of the ruling influences the measurement. The use of a coherent source is also considered in this case, but in this paper the synchronous phase detection procedure proposed in [Yatagai 1984] and [Omura 1988] is adopted, instead of the linear conversion of intensity to phase previously proposed. When using a white light converging source a five step phase-shifting algorithm designed for use in interferometry is used, instead of the previously proposed direct conversion from intensity to phase. The experimental setup, however, remains the same in order to take advantage of the properties of the source's coherence function.

Their main conclusions are the better visibility of the fringes when using non-coherent sources (as they reduce high order diffractive effects), and how the quality of the measurement is severely degraded for large shear values, meaning high-frequency gratings. Lateral shears of 1/40 of an aperture with unit radius are proposed for the

particular surface under test. Measurements using 200lpi and 300lpi rulings (with 0.127mm and 0.085mm period, respectively) are said to present accuracy problems in the final surface reconstruction, whereas when using a 1000lpi grating the diffractive effects in the ronchigram are so great that even fringe visibility is severely degraded.

In the latest approach we are aware of, a new setup was presented in order to reduce the high-order terms caused by diffraction in the Ronchi test [Hibino 1997]. It is shown how the high order diffractive terms are bound to appear in the recorded ronchigrams, either by the use of a square-wave transmittance ruling or by the high order terms present in any real-world sinusoidal transmittance ruling, which are called quasi-sinusoidal rulings. These unexpected terms are measured for a sinusoidal intensity pattern recorded by the authors using interferometric techniques. The experimental setup is quite similar to the one used by [Yatagai 1984], but a rotating ground glass diffuser is used as a screen, prior to recording the intensity pattern using a CCD detector (Fig.5.2.8).

Fig.5.2.8.- Experimental setup for [Hibino 1997]

where L_1 is the test lens, G a quasi-sinusoidal grating, L_2 an imaging lens and D a rotating ground glass diffuser. C is the CCD detector.

Apart from the smoothing process caused by the speckle that appears after the light crosses the rotating diffuser, the high order non-sinusoidal terms are suppressed up to their *n* term by using a tailored phase-shifting algorithm with *n*+2 samples. Two ronchigrams recorded in perpendicular directions of the Ronchi ruling are needed in order to obtain a surface reconstruction by integration using the least squares fitting method. Spherical wavefronts of 9.9λ are claimed to be measured with errors of 0.014λ. However, the application has not been tested on surfaces where a high amount of aberration was to be measured.

To summarize the reported works on the application of phase-shifting techniques to the Ronchi test, we could therefore point out that:

- The techniques presented tackle the presence of high order diffraction terms in the recorded intensity pattern in different ways. All the techniques tend to reduce the recorded intensity patterns to sinusoidal shapes through a) approximation; b) using the coherence properties of a non-monochromatic extended source; or c) using a rotating ground glass diffuser in order to smooth the recorded pattern combined with a tailored phase-shifting algorithm.
- The technique used in [Yatagai 1984] and [Omura 1988] is based on the assumption of ideal rulings where no even order terms appear in the Fourier series development of the ruling transmittance. Furthermore, any higher order terms are neglected in front of the first derivative term. However, in an ideal binary grating the 11^{th} order harmonic signal is 9% of the fundamental frequency signal, which may be considered an important error source in some applications. The technique was applied to aspherical and spherical surfaces.
- The technique put forward in [Wan 1990] and [Wan 1993] can measure both great and small amounts of aberration, meaning that it is capable of measuring both spherical and aspherical surfaces. However, its use of non-monochromatic extended sources with variable coherence degrades the fringe visibility to some extent, which causes an undesired increment in the random noise recorded.
- The work by [Hibino 1997] is the most realistic when dealing with the presence of high-order terms. However, the tailored phase-shifting algorithm used (a seven-sample algorithm) compensates for odd harmonic terms only up to the 5th harmonic of the frequency of the ruling. The additional smoothing introduced by the speckle appearing as the light travels through the rotating ground glass diffuser may account for the higher order diffraction terms in case of slightly deformed wavefronts like the one presented (10λ defocusing in a spherical wavefront), but no information is provided on what would happen when introducing important alterations in the curvature of the wavefront under test.
- None of the techniques presented tackles the problem of measuring non-rotationally symmetric surfaces, such as toroidal ones. Only the technique in [Wan 1993] tests a related topic, when measuring the amount of astigmatism present in a wavefront, by fitting the reconstructed wavefront to Zernicke polynomials.
- None of the techniques presented allows to us to foresee what would happen when applying them to toroidal surfaces, which have a very high inherent amount of non-

rotationally symmetric wavefront aberration. Yatagai's approximations are no longer valid in the presence of such amounts of aberration. The coherence function of the source used by Wan et al is optimized at a given spot area on the Ronchi ruling at which the fringes have a good contrast; this optimization occurs only at one shear position ($s=\lambda r/T$, with r radius of curvature), which depends on the radius of the surface being measured, so a toroidal surface will cause serious problems in obtaining good contrast fringes in the whole field of view. Finally, in our opinion it is not ensured that the smoothing from the speckle of a rotating diffuser, together with a suited phase-stepping algorithm that removes only up to the 5^{th} term, is enough to remove the diffractive high order terms from the signal when a toroidal surface is measured.

- None of the techniques presented therefore proposes an experimental setup satisfactory enough to reduce the complex intensity patterns resulting from the Ronchi test to sinusoidal patterns to which phase stepping procedures apply, when measuring non-rotationally symmetric surfaces.

5.2.2.2.- Application of phase-shifting techniques to non-sinusoidal, spatially stable intensity patterns

It has been shown that much of the research being carried out in the field is directed towards reducing the complex shapes of the recorded signals on the ronchigrams to sinusoidal shapes. However, the shape of the wavefront that will be measured when testing a toroidal surface is very likely to bring on great difficulties in reducing the complex signal from the shadow pattern to a sinusoidal signal, as this shape will depend on the difference of the two orthogonal radii of curvature that define the toroidal surface. In this section, a different approach will be discussed: instead of reducing the intensity patterns to sinusoidal ones in order to apply phase shifting procedures, a general method for developing phase shifting algorithms for non-sinusoidal signals will be presented [Arasa 1997].

Suppose that a general signal, with a form described by f(x), was obtained from the intensity pattern. Each single peak (corresponding to the intensity pattern of a bright line) may be described using a function $f_i(x)$, and assigned a null value at the points outside the peak. Thus,

$$f(x) = \sum_{i=1}^{P} f_i(x) \qquad (5.2.21)$$

in a signal where P peaks are present in the intensity pattern. Only one-dimensional signals are considered, as the transmittance of the Ronchi ruling is assumed to vary as a square wave along the X axis, and differences between consecutive pixels in the Y axis direction, i.e. along the ruling stripes, should be very small even in the event of large amounts of aberrations being present. This assumption will be seen to have little significance at the end of this section.

Each function $f_i(x)$ may be described as a Fourier series; not writing the dependence on x of $\Phi(x)$, this series would be

$$f_i(x) = \frac{a_0}{2} + \sum_{k=1}^{\infty} a_k \cos(k\Phi) + \sum_{k=1}^{\infty} b_k \operatorname{sen}(k\Phi) \qquad (5.2.22)$$

with a_k and b_k described as

$$a_k = \frac{2}{T}\int_0^T f_i(x)\cos\left(\frac{2\pi n x}{T}\right)dx \qquad (5.2.23)$$

$$b_k = \frac{2}{T}\int_0^T f_i(x)\operatorname{sen}\left(\frac{2\pi n x}{T}\right)dx \qquad (5.2.24)$$

When a phase stepping procedure is applied, the j intensity pattern has a phase increment α_j relative to the phase of the first measurement, so

$$f_i(x+\alpha_j) = a_0 + \sum_{k=1}^{\infty} a_k \cos\left(k(\Phi+\alpha_j)\right) + \sum_{k=1}^{\infty} b_k \operatorname{sen}\left(k(\Phi+\alpha_j)\right) \qquad (5.2.25)$$

The measured intensity pattern, introducing the fringe modulation and the ground noise level, will thus be, at each pixel

$$I_j = I_o\left\{1+\gamma\cdot f_i(x_{pixel})\right\} = I_o\left\{1+\gamma\cdot\left[a_0 + \sum_{k=1}^{\infty} a_k \cos\left(k(\Phi+\alpha_j)\right) + \sum_{k=1}^{\infty} b_k \operatorname{sen}\left(k(\Phi+\alpha_j)\right)\right]\right\} \qquad (5.2.26)$$

After some algebra, the expression may be written as

$$I_j = I_0 + \gamma\cdot I_0\cdot\frac{a_0}{2} + \qquad (5.2.27)$$

$$+\sum_{k=1}^{\infty}\gamma\cdot I_0\cdot\left[a_k\cos(k\Phi)+b_k\operatorname{sen}(k\Phi)\right]\cos\left(k\alpha_j\right) + \sum_{k=1}^{\infty}\gamma\cdot I_0\cdot\left[-a_k\operatorname{sen}(k\Phi)+b_k\cos(k\Phi)\right]\operatorname{sen}\left(k\alpha_j\right)$$

which may be rewritten as

$$I_j = \mu_0 + \sum_{k=1}^{\infty}\mu_k\cos\left(k\alpha_j\right) + \sum_{k=1}^{\infty}\eta_k\operatorname{sen}\left(k\alpha_j\right) \qquad (5.2.28)$$

or, including the zero order inside the sum

$$I_j = \sum_{k=0}^{\infty} \mu_k \cos(k\alpha_j) + \sum_{k=1}^{\infty} \eta_k \operatorname{sen}(k\alpha_j) \qquad (5.2.29)$$

provided that we define

$$\mu_0 = I_0 + \gamma \cdot I_0 \cdot \frac{a_0}{2} \qquad (5.2.30)$$

$$\mu_k = \gamma \cdot I_0 \left[a_k \cos(k\Phi) + b_k \operatorname{sen}(k\Phi) \right] \qquad (5.2.31)$$

$$\eta_k = \gamma \cdot I_0 \left[-a_k \operatorname{sen}(k\Phi) + b_k \cos(k\Phi) \right] \qquad (5.2.32)$$

A least squares technique will now be applied supposing that a number J of measuring steps are available in a given experimental setup. In order to apply the least squares technique a finite number of terms in each summation is required. If each sum was extended from 0 to N, J>2N+1 would have to be accomplished. That is, extending the sums up to the fifth harmonic in the series would require a minimum of twelve experimental recordings at different phase shifts. Once this condition is satisfied, the function to minimize would be

$$\Im(\mu_k, \eta_k) = \sum_{j=1}^{J} \left[I_j - \sum_{k=0}^{N} \mu_k \cos(k\alpha_j) - \sum_{k=1}^{N} \eta_k \operatorname{sen}(k\alpha_j) \right]^2 \qquad (5.2.33)$$

$$\frac{\partial \Im(\mu_k, \eta_k)}{\partial \eta_m} = \sum_{j=1}^{J} 2 \cdot \left[I_j - \sum_{k=0}^{N} \mu_k \cos(k\alpha_j) - \sum_{k=1}^{N} \eta_k \operatorname{sen}(k\alpha_j) \right] \cos(m\alpha_j) = 0 \qquad (5.2.34)$$

$$\frac{\partial \Im(\mu_k, \eta_k)}{\partial \eta_m} = \sum_{j=1}^{J} 2 \cdot \left[I_j - \sum_{k=0}^{N} \mu_k \cos(k\alpha_j) - \sum_{k=1}^{N} \eta_k \operatorname{sen}(k\alpha_j) \right] \operatorname{sen}(m\alpha_j) = 0 \qquad (5.2.35)$$

With the assumed conditions, J=12 and N=5. Keeping N and J in the equations in order to make them more general, this yields a set of equations

$$\sum_{j=1}^{J} I_j \cos(m\alpha_j) = \sum_{j=1}^{J} \sum_{k=0}^{N} \mu_k \cos(k\alpha_j) \cos(m\alpha_j) + \sum_{k=1}^{N} \eta_k \operatorname{sen}(k\alpha_j) \cos(m\alpha_j) \qquad (5.2.36)$$

$$\sum_{j=1}^{J} I_j \operatorname{sen}(m\alpha_j) = \sum_{j=1}^{J} \sum_{k=0}^{N} \mu_k \cos(k\alpha_j) \operatorname{sen}(m\alpha_j) + \sum_{k=1}^{N} \eta_k \operatorname{sen}(k\alpha_j) \operatorname{sen}(m\alpha_j) \qquad (5.2.37)$$

which may be written using a matrix notation as

$$\begin{pmatrix} \sum_{j=1}^{J} I_j \\ \sum_{j=1}^{J} I_j \cos(\alpha_j) \\ \sum_{j=1}^{J} I_j \cos(N\alpha_j) \\ \sum_{j=1}^{J} I_j \operatorname{sen}(\alpha_j) \\ \dots \\ \sum_{j=1}^{J} I_j \operatorname{sen}(N\alpha_j) \end{pmatrix} = \begin{pmatrix} 1 & \sum_{j=1}^{J} \cos(\alpha_j) & \dots \\ \sum_{j=1}^{J} \cos(\alpha_j) & \sum_{j=1}^{J} \cos(\alpha_j) & \dots \\ \dots & \dots & \dots \\ \sum_{j=1}^{J} \cos(N\alpha_j) & \sum_{j=1}^{J} \cos(\alpha_j) & \dots \\ \sum_{j=1}^{J} \operatorname{sen}(\alpha_j) & \sum_{j=1}^{J} \operatorname{sen}(\alpha_j)\cos(\alpha_j) & \dots \\ \dots & \dots & \dots \\ \sum_{j=1}^{J} \operatorname{sen}(N\alpha_j) & \sum_{j=1}^{J} \operatorname{sen}(N\alpha_j)\cos(\alpha_j) & \dots \end{pmatrix} \quad (5.2.38)$$

$$\begin{pmatrix} \sum_{j=1}^{J} \operatorname{sen}(\alpha_j) & \dots & \sum_{j=1}^{J} \operatorname{sen}(N\alpha_j) \\ \sum_{j=1}^{J} \cos(\alpha_j)\operatorname{sen}(\alpha_j) & & \sum_{j=1}^{J} \cos(\alpha_j)\operatorname{sen}(N\alpha_j) \\ \dots & & \\ \sum_{j=1}^{J} \cos(N\alpha_j)\operatorname{sen}(\alpha_j) & & \sum_{j=1}^{J} \cos(N\alpha_j)\operatorname{sen}(N\alpha_j) \\ \sum_{j=1}^{J} \operatorname{sen}^2(\alpha_j) & & \sum_{j=1}^{J} \operatorname{sen}(\alpha_j)\operatorname{sen}(N\alpha_j) \\ \dots & & \\ \sum_{j=1}^{J} \operatorname{sen}(N\alpha_j)\operatorname{sen}(\alpha_j) & & \sum_{j=1}^{J} \operatorname{sen}^2(N\alpha_j) \end{pmatrix} \cdot \begin{pmatrix} \mu_0 \\ \mu_1 \\ \dots \\ \mu_n \\ \eta_1 \\ \dots \\ \eta_n \end{pmatrix}$$

or, naming the matrices properly

$$\mathbf{I} = \mathbf{A} \cdot \mathbf{M} \qquad (5.2.39)$$

The phase information we are trying to retrieve from the signal is now only in matrix M; so, each of the μ_k and η_k values may be determined through

$$\mathbf{M} = \mathbf{A}^{-1} \cdot \mathbf{I} \qquad (5.2.40)$$

and $\Phi(x)$ may be obtained from combinations between μ_k and η_k, such as

$$\operatorname{tg}[k\Phi] = \frac{\frac{\mu_k}{\eta_k} \cdot \frac{b_k}{a_k} - 1}{\frac{\mu_k}{\eta_k} + \frac{b_k}{a_k}} \qquad (5.2.41)$$

An example of the described procedure will be provided, from an experimental measurement carried out in the experimental setup described in Section 4.1. This example is presented to show the kind of results that the described procedure may produce. The surface tested was spherical and the test was carried out using a 25.4lpi ruling (1mm period). No physical interaction models on the signal need to be considered, as the model is based on the shape of the registered signal. Fig. 5.2.9 shows the recorded intensity pattern for a 148mm radius of curvature concave surface of a spherical ophthalmic lens whose first convex surface was ground in order to make it optically inactive, as explained in Section 4.1. Four fringes were visible in the central region of the image, corresponding to the four peaks visible in Fig.5.2.9. These will be referred to as peaks 1, 2, 3 and 4, starting with the peak with its center at a lower pixel number (left to right in the figure).

Fig.5.2.9: Measured intensity pattern in the Ronchi test setup applied to a spherical surface. The surface has a radius of curvature of 148mm and the Ronchi test has a period of 1mm.

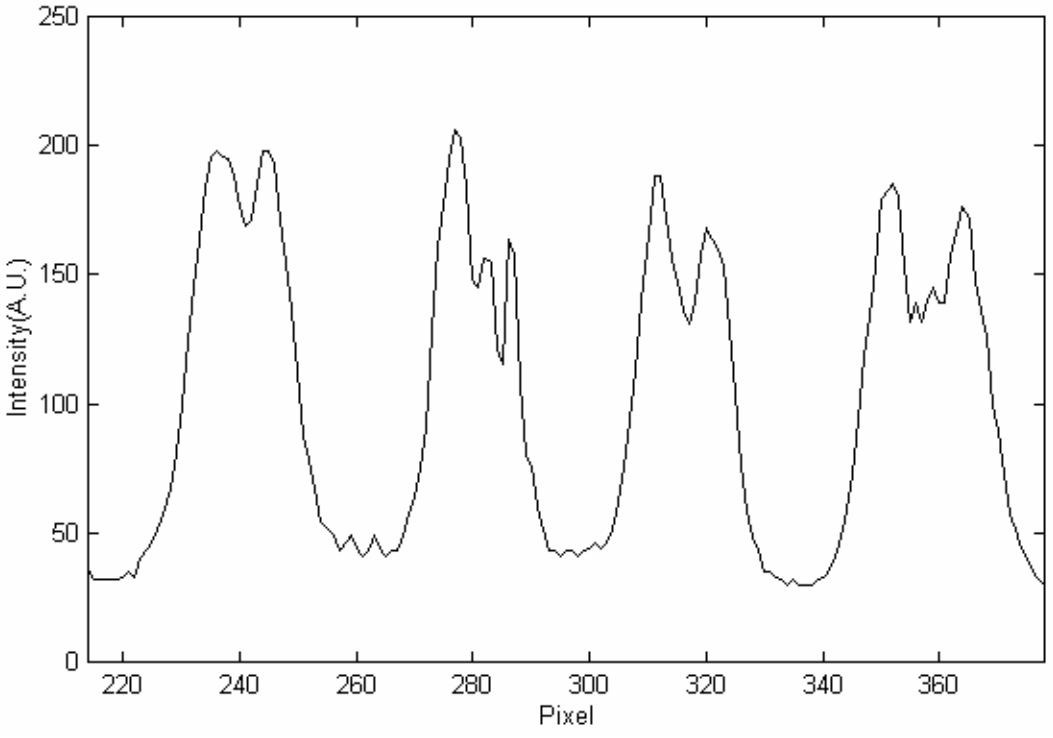

A function for $f_i(x)$ must be considered at each peak. Prior to this procedure, each peak was normalized to the noise level, leaving a signal from zero to unity. In this case, the shape of the intensity pattern suggested that the difference of two Gaussian curves was well suited to the signal. The shape of the signal was given, for each peak, for the expression:

5.27

$$f_i(x) = a_i + b_i e^{-\frac{(x-c_i)^2}{2d_i^2}} - e_i e^{-\frac{(x-f_i)^2}{2g_i^2}} \qquad (5.2.42)$$

After dividing the intensity pattern in order to treat each peak alone, the peaks were normalized in both their horizontal and vertical dimensions. Each peak was then curve-fitted to the function in Eq.5.2.42 in order to obtain numerical values for coefficients from a to g. Table 5.2.1 presents the values obtained for each of the peaks, together with the correlation coefficient values (r^2) and their standard deviation (σ^2). This fitting provides us with a theoretical shape for the measured signal, and was carried out using commercially available software (TableCurve© 2D).

Table 5.2.1: Coefficients and quality of the fit of Eq.5.2.42 to the peaks in Fig.5.2.9

	a_i	b_i	c_i	d_i	e_i	f_i	g_i	r^2	s^2
Peak#1 i=1	0.042	1.789	0.549	0.121	1.012	0.552	0.068	0.996	0.0243
Peak#2 i=2	0.056	2.013	0.544	0.137	1.404	0.552	-0.081	0.991	0.0369
Peak#3 I=3	0.066	6.443	0.532	0.111	5.870	0.534	-0.097	0.993	0.0304
Peak#4 i=4	0.033	6.754	0.529	0.129	6.189	0.530	-0.112	0.993	0.0312

Once $f_i(x)$ is known at each peak, we will obtain its Fourier transform. The fitted signal is needed in order to avoid the inclusion of deviations from the expected shape in the Fourier spectrum of the signal as far as possible. As the procedure is identical for the four peaks present in Fig.5.2.9, only the results for peak #2 will be presented. Peak #2 was selected because of its particular shape, which yields interesting results in the measured phase of the signal. However, the procedure was applied to the whole signal, and complete phase results for the four peaks will be presented next.

The limit in the number of terms of the Fourier series was chosen as 11. This means that terms up to the fifth harmonic are considered, which yield suitable signal reconstructions, as may be seen in Fig. 5.2.10b. In another trials, 21 terms (up to the tenth harmonic) were considered, showing a sum of the Fourier series resembling the original signal more closely, specially at the peak horizontal edges. However, the increase in calculation time (a 21X21 matrix appeared in the calculations), together with the need for 21 equivalent displacements in one single period of the ruling, made

us select just eleven terms in the series. Notice, however, that no fundamental limitation in the presented equations prevents from using more terms in the series.

As a least squares technique must be applied, we need a minimum of 12 experimental measurements to account for our 11 unknowns. A phase increment of T/11 (91μm) was chosen, and 12 measurements will be made, so the first and last experimental measurements will be exactly one period apart.

Fig. 5.2.10: Peak #2: (a) Normalized experimental measurement and (b) Fourier series reconstruction of (a) with terms up to the fifth harmonic

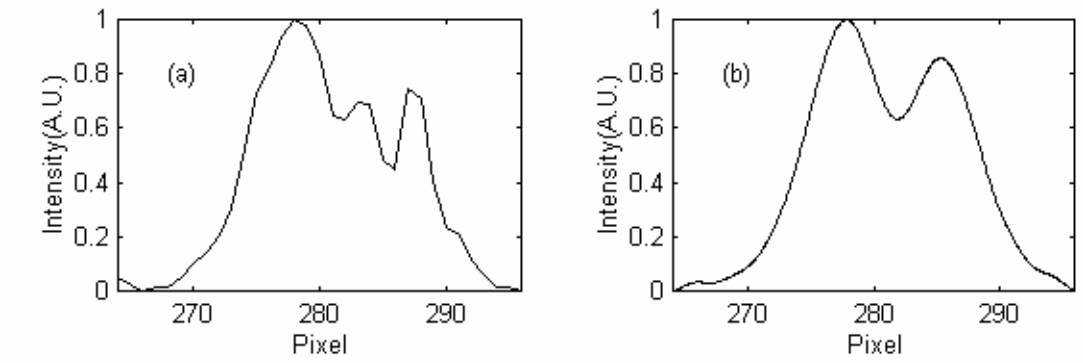

Eq.5.2.31 and Eq.5.2.32 then apply to calculate the μ_κ and η_k values, from which values for the phase, and the modulation of the signal may be obtained. Such values are presented in Fig. 5.2.11 for peak #2. Notice how the deviations from the fitted shape of the signal cause major phase deviations from the linear theoretical value that would be expected under ideal conditions. Notice also how this deviation may even be appreciated in the modulation values, slightly different in the area where the measured signal deviates from the fitted one.

Fig. 5.2.11: Peak #2: (a) Reconstructed phase of this peak; (b) Measured modulation

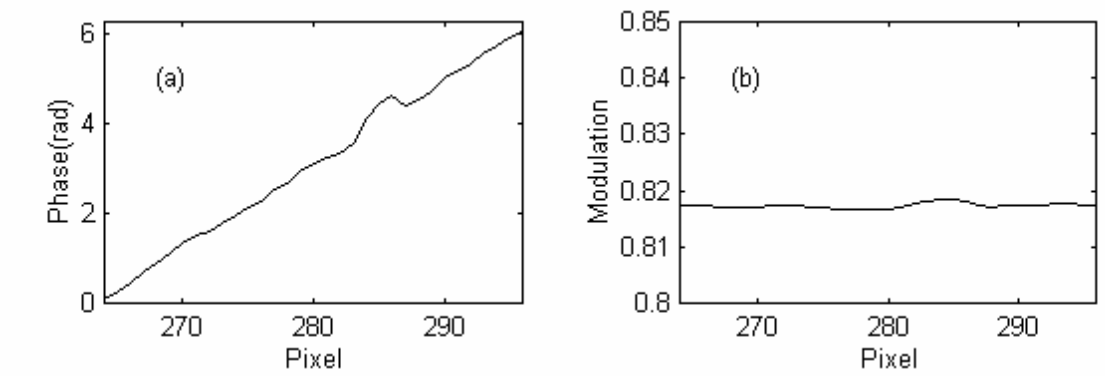

Working on the three remaining peaks in the same way, a phase value may be obtained for each pixel considered. This lets us obtain the wrapped phase, which closely resembles the one obtained in Fig.5.2.2, obtained when developing an interferometric theoretical example. The wrapped and unwrapped phase values for all the peaks in Fig.5.2.9 are presented in Fig.5.2.12. Once the unwrapped phase is obtained, a wavefront reconstruction procedure together with a fitting to a set of Zernicke polynomials would yield the measured shape of the wavefront.

Fig. 5.2.12: All peaks; (a) Wrapped phase; (b) Unwrapped phase for the signal in Fig. 5.2.9.

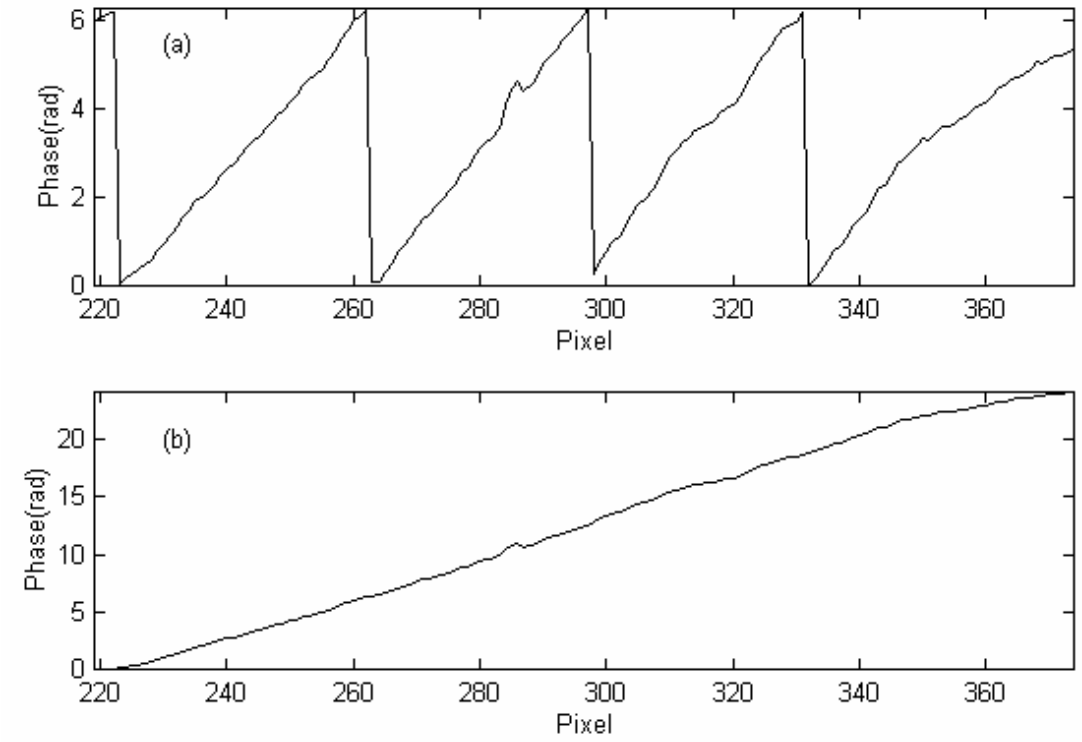

We are aware of the many possible drawbacks of the technique presented. In particular, a detailed study of the accuracies involved, and of how much information is lost either along the fitting step or when deciding the number of terms included in the Fourier sum would be very useful. However, there is an underlying assumption concealed throughout the development described: the signal presented must be spatially stable. That is, if we look at each independent pixel, and at the signal variation it experiences, all the pixels in one peak (at least) should undergo the same kind of variation along one period.

This signal variation depends very much on the shape of the incident wavefront. The local curvature of the incident wavefront when impinging on the edges of the

stripes of the Ronchi ruling plays a key role in the amount of diffractive effects that will be present in the analyzed signal. As a three-dimensional wavefront hits a plane ruling, the local curvature of the wavefront at each ruling line and along each of the ruling lines will change smoothly along the ronchigram even for perfect wavefronts. The change of the local curvature will yield alterations in the signal shape, so the signal will not be spatially stable, as it will vary smoothly. If the signal shape does not stay constant throughout one period of the ruling (that is, throughout the phase shifting of one single peak), procedures based on using this shape are obviously not reliable, as they would mean a priori knowledge of the shape of the wavefront being measured. These considerations led us to abandon phase shifting procedures in order to improve the measurements, and to adopt the microstepping procedure presented in Section 5.3.

However, before describing these microstepping procedures, which will yield the final approach to better measurements using the Ronchi test, Section 5.2.3 will use experimental ronchigrams to show how the shape of the registered signal is altered when the Ronchi ruling is moved during the different phase-shifting steps, ruling out the possibility of using phase-shifting schemes in the Ronchi test technique.

5.2.3.- Validity of phase-shifting techniques applied to the Ronchi test

Up to this point, the treatment presented in Section 5.2.2.2 of the non-sinusoidal signals obtained using the Ronchi test technique would allow to obtain full phase reconstructions resembling those obtained in interferometry. The performance of such a treatment comes down to a problem involving the experimental ability to produce small displacements and the computing power and speed needed to perform the calculations.

However, as pointed out above, an assumption has been made about the signal; as in the case of interferometry, the signal must remain the same throughout the phase-stepping procedure. That is, the value of the intensity pattern at each particular point may change, but the signal must continue to be described by the same function (a sine in interferometric measurements, or each of the $f_i(x)$ fitted at each of the intensity peaks in the Ronchi test). This means that each of the measured pixels should undergo the same kind of intensity variation throughout the phase stepping process (under experimental limits). That is, the signal must be spatially stable [Arasa 1997b].

A theoretical example will show this spatial stability of the signal when interferometric techniques are used. A general signal of the shape

$$I_i(x) = 0.5 \cdot \left[1 + \cos(\Phi(x) + \alpha_i)\right] \qquad (5.2.43)$$

was calculated supposing a total phase variation of two fringes along 100 pixels. Eleven phase steps were performed, with a phase increment of $\Delta\alpha = 2\pi/11$ rad between them. This means that the received signal in the first measurement step would be the one presented in Fig.5.2.13, which has a variation of two complete periods.

Fig.5.2.13: Theoretical interferometric intensity signal in the first measuring step.

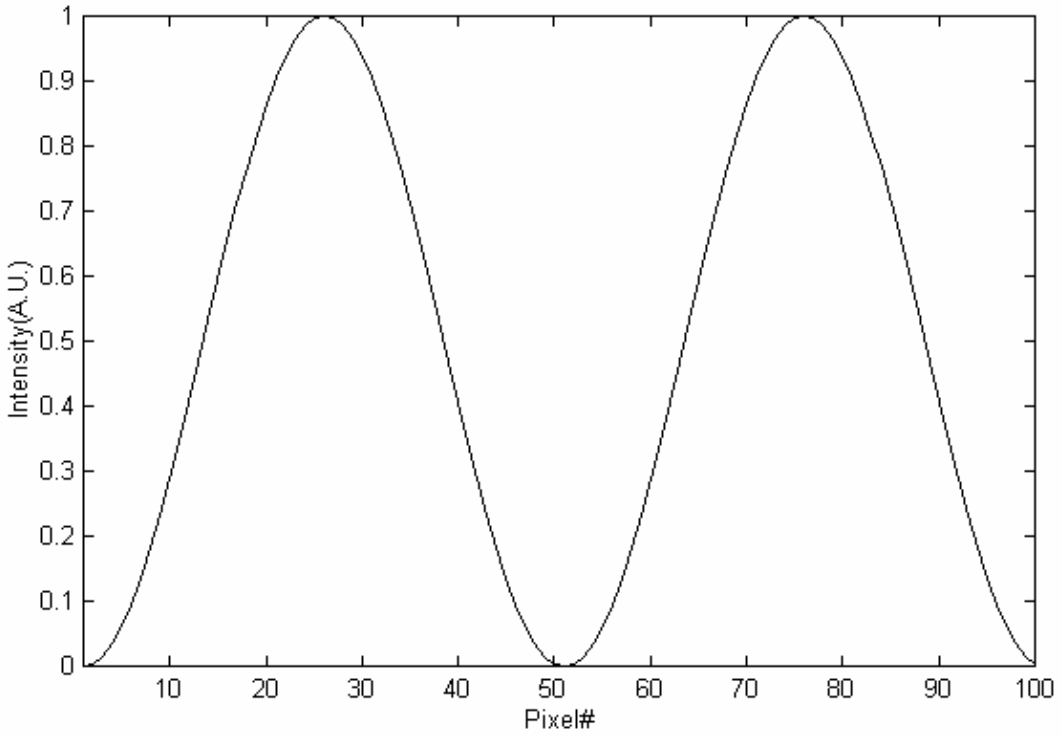

When the phase-stepping procedure is applied, with twelve displacements with $\Delta\alpha = 2\pi/11$ rad, each single pixel in the image will undergo intensity variations that will follow the signal variations. This means that each of the pixels in the image will undergo the same kind of variation, with the only difference that the signal will start at a different point at each pixel, because of their different initial value in the first intensity pattern. That is, each pixel has a different initial phase value. If we plotted the intensity variation at a given pixel as a function of the number of steps, instead of the intensity pattern for a given step at all pixels, we would see how its intensity had varied during the phase-shifting procedure. Fig. 5.2.14 shows these intensity variations over one of the theoretical interferometric peaks, at pixels numbers (a) 1; (b) 7; (c) 13; (d) 18; (e) 24; (f) 30; (g) 36; (h) 42 ; and (i) 48 of Fig. 5.2.13 after a simulated phase-stepping procedure was performed. All Y axes represent intensity in arbitrary units, whereas all X axes represent the step number. Its shape is clearly that of a cosine, with different

starting points depending on the initial phase of the pixel. It must be stressed that only one period variation is observed, as the phase-shifting steps were carried out during a single period.

Fig. 5.2.14: Intensity variations at fixed pixels when a phase stepping procedure over one period is applied. The pixels are numbers (a) 1; (b) 7; (c) 13; (d) 18; (e) 24; (f) 30; (g) 36; (h) 42 ; and (i) 48 of Fig. 5.2.13. Y axes represent intensity in arbitrary units; X axes represent step numbers

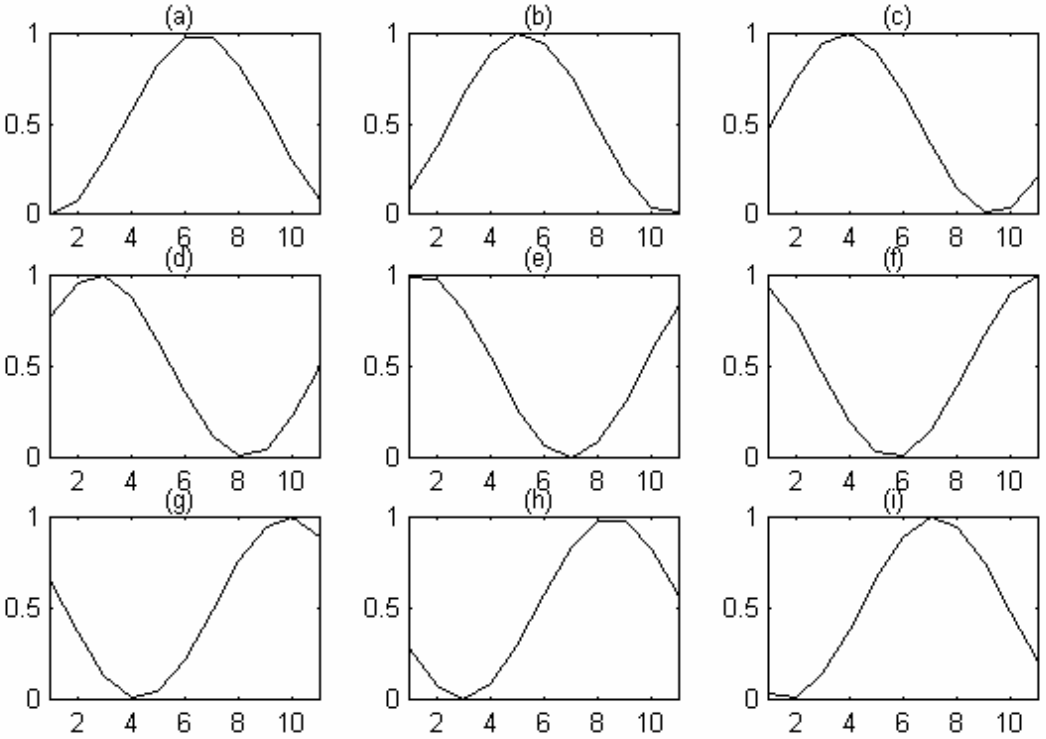

A three-dimensional representation summarizing Fig. 5.2.13 and Fig. 5.2.14, and including all intensity measurements is also possible (Fig. 5.2.15). The pixel number was placed along the X axis, the step number along the Y axis and the intensity in arbitrary units along the Z axis. Both three-dimensional (Fig.5.2.15a) and two-dimensional grayscale plots (Fig.5.2.15b) are provided.

We will now look at what happens when the same analysis is performed on the shadow pattern obtained using the Ronchi test to sample the wavefront. We will apply the analysis carried out for interferometric measurements to the same four-peaked signal present in Fig.5.2.9. Measurements will be carried out with the experimental data used in Section 5.2.2.2. Peaks 3 and 4 of Fig.5.2.9 are arbitrarily selected for the analysis, as any part of the signal gives rise to comparable results.

Fig. 5.2.15: Intensity variations versus pixel number and step number for theoretical interferometric measurements. (a) Three-dimensional surface plot and (b)Two-dimensional grayscale plot.

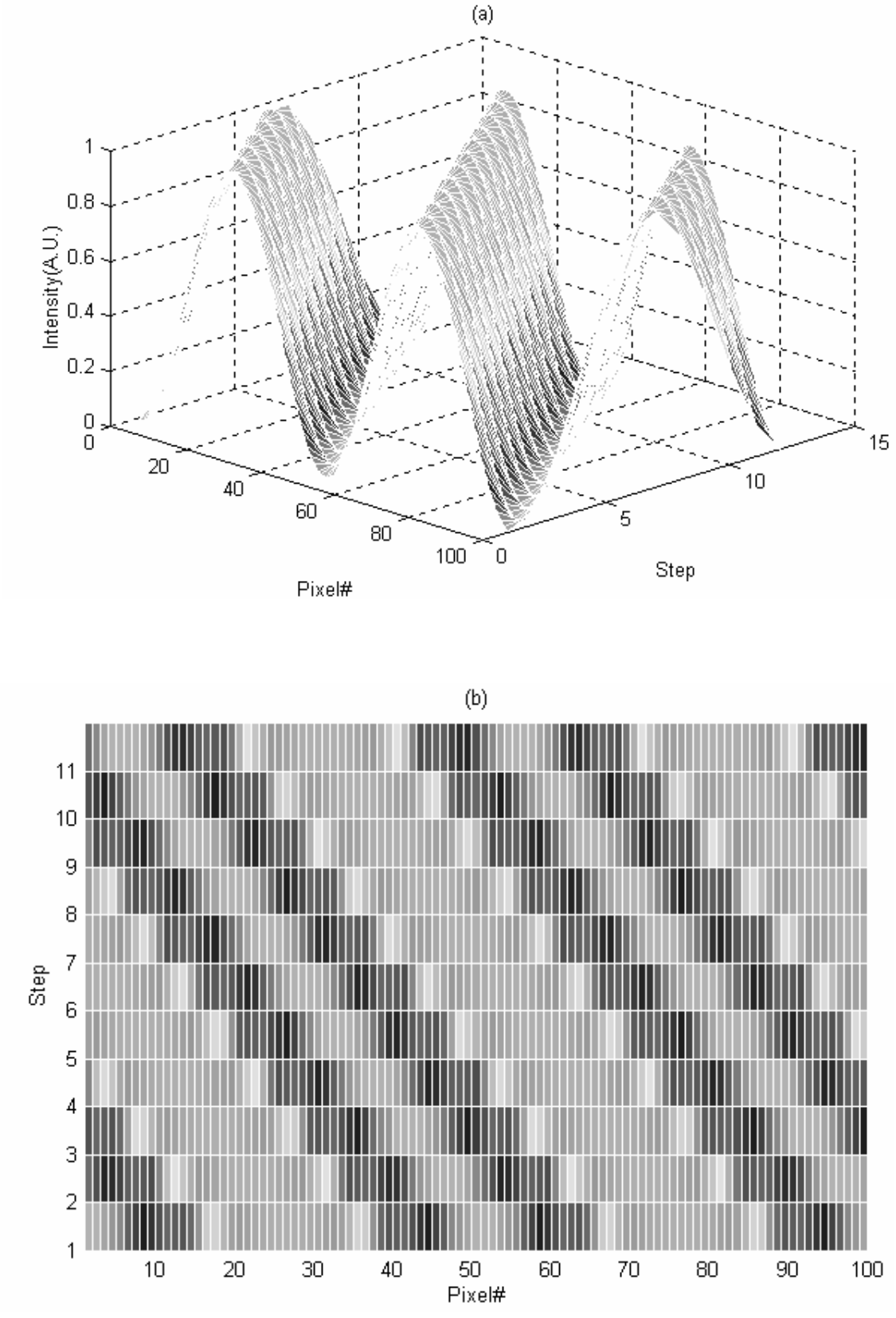

Fig. 5.2.16: Intensity variations at fixed pixels in the fourth peak of Fig. 5.2.9 when a phase-shifting procedure over one period is applied. The pixels are numbers (a) 332; (b) 337; (c) 342; (d) 347; (e) 352; (f) 357; (g) 362; (h) 367; and (i) 372. All Y axes represent intensity in arbitrary units; all X axes represent step numbers.

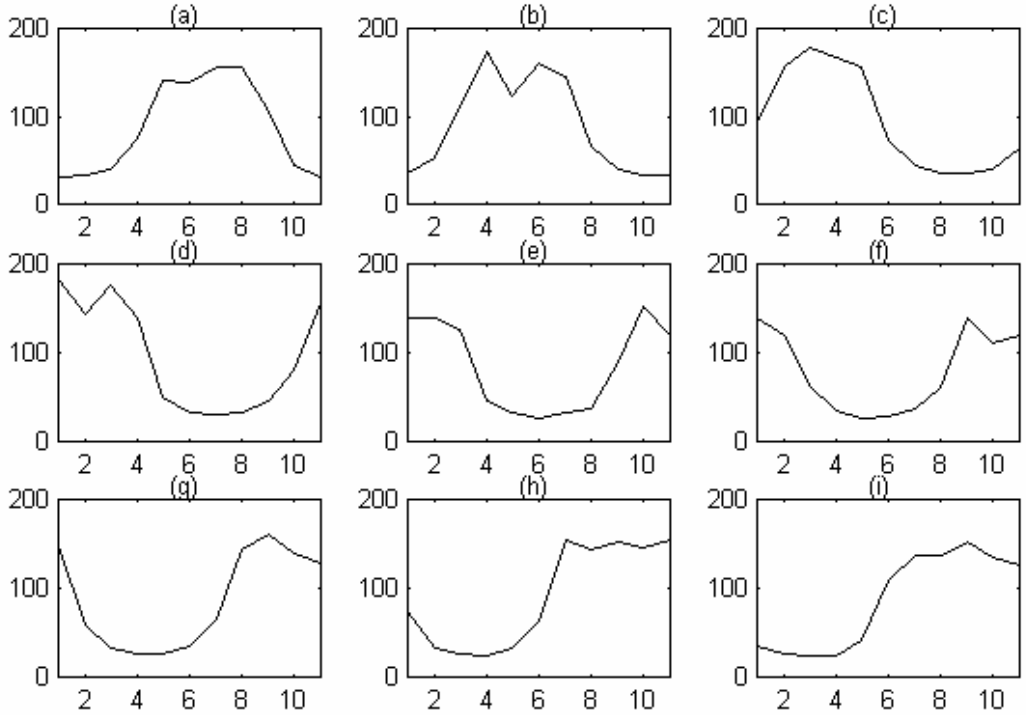

Fig.5.2.16 shows the intensity variations at each pixel of the signal corresponding to the fourth peak of Fig. 5.2.9 during the phase-stepping procedure. As in Fig. 5.2.14, all Y axes stand for intensity in arbitrary units, and X axes represent the number of phase increments carried out. The corresponding pixel numbers from Fig. 5.2.9 are (a) 332; (b)337; (c) 342; (d) 347; (e) 352; (f) 357; (g) 362; (h) 367 ; and (i) 372. The pixel spacing between the different subplots in the graph has been kept intentionally constant in order to show the variations in signal shape better. Only intensity values at eleven step increments are shown, as the 12^{th} measured value coincides with the first measured value except for very small intensity fluctuations that will not affect the conclusions we reach.

It is easily seen how the variations in signal shape do not only depend on the value of the pixel in the first measurement. The pixels in Fig. 5.2.16b and Fig. 5.2.16h, for instance, describe different intensity variations during the complete step cycle. It must be noticed here that no assumptions whatsoever have been made about the signal shape, as the graphs presented are obtained from experimental intensity variations within the phase stepping process.

In Fig. 5.2.17 the three-dimensional graph of intensity versus pixel number and step number shows the great irregularity present in the signal at the intensity maxima. In order to closely resemble the simulated interferometric measurement of Fig.5.2.15, now the intensity values of peak #3 and peak #4 in fig.5.2.9 have been represented against the pixel number and the number of steps performed. Deviations from the expected uniform behaviour as the phase-shifting steps are performed become evident in fig.5.2.17b, where the intensity maxima of the peaks may be seen to increasingly narrow.

These irregularities, as mentioned in the last paragraph of Section 5.2.2.2, are caused by variations in the diffractive behavior of the test introduced by the interaction between the wavefront and the Ronchi test stripes. Even at low frequencies such as the one presented (the shear value for the first diffracted order is in this case only 15.9μm, which amounts to a shear-to-period ratio of .016, small enough to consider the diffractive and geometrical models of the Ronchi test as equivalent -see Sections 3.2.2 or 5.1-), diffractive terms vary depending on the curvature of the incident wavefront, giving rise to such great alterations in the intensity pattern that the measured signal depends on the position of the ruling.

At this point, a fundamental difference from interferometric techniques may be pointed out, which comes forward as the reason for these alterations in the shape of the signal. In interferometric techniques the phase step is introduced through modifying the reference wavefront; the resulting wavefront is then accurately measured because of the amount of additional information obtained in the phase-stepping process. Incidentally, in the Ronchi test technique the wavefront to be measured is sampled through the Ronchi ruling; the ruling displacements may therefore be stepped in order to get more information on the measured wavefront. There is no reference wavefront to step. As the interaction of the ruling with the wavefront changes when the ruling is displaced, the measured signal is altered by small amounts at each step. This interaction depends on the shape of the wavefront being measured, so only configurations where the diffractive components may be neglected (with intelligent experimental setups [Hibino 1997] or through approximation [Omura 1988])) will permit the application of phase measurement techniques to the Ronchi test. These configurations, however, have their particular limitations, as pointed out in Section 5.2.2.1.

Fig. 5.2.17: Intensity variations of peaks 3 and 4 versus pixel number and step number. (a) Three-dimensional surface plot and (b) Two-dimensional grayscale plot.

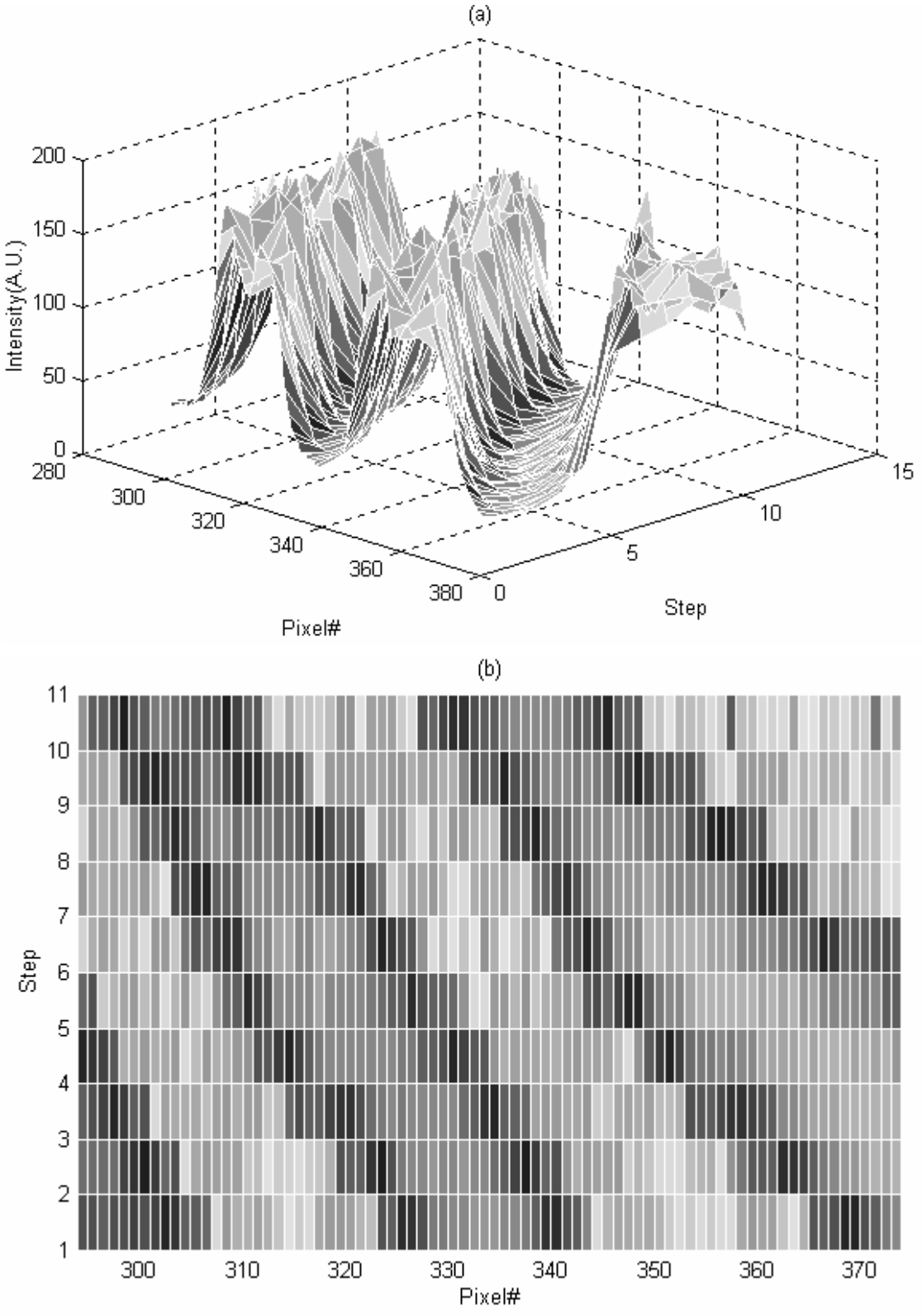

Our conclusion is that, even at low frequencies, diffraction caused by the edges of the ruling alters the wavefront being measured. If this alteration were the same along the displacement of the ruling which introduces the phase steps, phase-stepping procedures might be applied, as explained in Section 5.2.2.2. However, these diffractive terms alter the shape of the signal in a way that depends on the positions of the stripes of the ruling, and on the local curvature of the incident wavefront impinging on each stripe. That is, the local shape of the wavefront being measured alters the registered signal, which in a phase-shifting procedure would be used in order to obtain the aforementioned shape. This means that phase-shifting techniques are not likely to be applied to the Ronchi technique unless diffractive effects are eliminated in some way.

To sum up, in Section 5.2 it has been shown that although phase-shifting techniques appear to be a very good option for improving the Ronchi test accuracy without altering its very good dynamic range, fundamental limitations caused by the different diffractive behavior of the test depending on the local shape of the incident wavefront prevent them from being applied to the Ronchi test unless the diffractive terms in the signal are reduced or averaged to some extent. A method for performing phase measurements of spatially stable non-sinusoidal signals has also been proposed in Section 5.2.2.2.

5.3 Microstepping

Up to now , our efforts to improve the measurements made with the Ronchi test technique have failed. The common cause of failure for both the technique of increasing the frequency of the ruling that samples the wavefront, proposed in Section 5.1, and phase-shifting procedures, proposed in Section 5.2, was the presence of diffractive effects in the shadow pattern registered in the ronchigram. In this section a technique allowing an increase in the measured data points without the need for modifying the experimental setup described in Section 4 will be presented.

5.3.1.- Increasing the number of registers

The methodology presented for measuring surface topographies in Section 4.2, whose performance we are trying to enhance, was based on geometrical optics principles, as the slope and position of the wavefront were measured at a number of

points on the Ronchi test plane. These values were ray-traced to the tangent plane to the sample surface and yielded the value of the local normal at a set of its points given the position of the point light source was provided. Using this approach, only the position of the centers of the bright lines of the ronchigram is considered, and no information is needed from regions outside this center. This means that, if N different bright lines are found inside each of the orthogonal shadow patterns, a maximum of N^2 points on the surface may be measured.

The ideal solution for improving this technique would be one which preserved the geometrical interpretation of the Ronchi test, keeping the first order diffractive shear under the proposed threshold values (see Section 3.2.2), but which increased the number of registered fringe maxima, so the number of measured data points could be also increased.

Our proposal is to take advantage of the encoder motors present in our experimental setup, which nominally allow displacements of the Ronchi ruling with up to 0.1μm accuracy. If a ruling whose diffractive effects could be ignored is displaced along the X or Y axis a fraction of its period, we will obtain a new set of shadow patterns, where obviously diffractive effects can still be ignored, as the period of the ruling remains the same. This new shadow pattern will provide us with additional information about the surface, as a new set of position and slope pairs along X and Y directions will have been measured.

As only the position of the center of the stripe shadows is to be considered, the set of points obtained at each of the displacements may be superimposed to yield a final composed image, where diffractive effects will not have been increased. By making k displacements in each direction with a Ronchi ruling with T period, we obtain the sampling of a ruling with T/k period without any disturbing increase of the diffractive effects caused by high frequency rulings.

Because of its stepping nature, and of the values of typical displacements, which will be shown to be about 10μm, we called the technique Ronchi ruling microstepping. We must stress that the technique is completely independent of the surface (wavefront) being tested, and so both rotationally symmetrical and non-symmetrical surface measurements can be enhanced in this way.

Implementation of microstepping techniques within the data processing outline presented in Section 4.2 is straightforward, as each of the shadow patterns is independently eroded to a one pixel-wide line pattern. Once all the skeletons of a measurement series along both perpendicular directions have been obtained, these

are composed in a single image giving the total set of measured data points on the Ronchi plane, from superimposing each of the lines along the X direction with each line taking the Y direction. All intersection points between the lines yield the set of four values (x_R, y_R, u, and v) needed to carry out the ray-tracing process backwards to the tangent plane to the surface, and to measure at that surface point the local normal to the surface. The number of sampled points in the wavefront is exponentially increased as the number of steps rises.

In a typical application, such as the ones presented in Sections 6 and 7 of this work, 50.8µm steps are applied to a Ronchi test with a 0.508mm period (50lpi). This yields ten measurement increments, i.e., nine additional lines of data points measured between each of the lines of the original shadow pattern. From our experience, typical Ronchi patterns with good fringe visibility have around 10 light and dark shadows. This means that from obtaining 10^2 measured points with a single capture along two perpendicular directions of the ruling (10x10lines), through microstepping techniques we will be obtaining 10^4 measured points from an array of 100x100 clear stripes in twenty ronchigrams.

5.3.2.- Limits to the proposed technique

Microstepping has the advantage of increasing at will the number of data points measured on the surface with a given Ronchi ruling, no matter what the shape of the surface tested is. However, a set of different experimental conditionings will limit the performance of the technique.

A first limitation lies in the displacement capability of the encoder motors. However, as stated above, micrometric displacements and repeatabilities are commonplace to modern encoders. This would allow 500 displacements within one single period of a ruling with 0.508mm period, which would yield a measured point at almost each of the 512x512 pixels of a typical image. The encoder resolution will thus pose hardly any problems.

The main limitation to the technique, however, is the amount of measured information that may be treated. As the number of points increases exponentially, the amount of data obtained may be so high that it loses its usefulness because of the computing time needed to complete a full reconstruction of the surface. Table 5.3.1 shows how the amount of information rises exponentially as the number of steps in the microstepping procedure is increased. A typical ronchigram with 10 bright lines in the shadow pattern along either the X or Y axis was considered as an example. The

amount of information handled in the process was considered in the following way: from each data point, four real values are obtained, to account for the position on the Ronchi plane (two values, x_R and y_R) and the slope of the wavefront in both directions (two values, u and v). Real numbers need four bytes each. So each data point needs 16 bytes in order to be stored. The time intervals for the calculations are real values in the first four columns, and have been extrapolated from the former in the last two columns.

Table 5.3.1: Increase in the number of measured line shadows, maximum number of valid data points and of amount of information of each case, as the number of steps in a microstepping procedure increases. Computing time values are estimated from typical measurements.

Nº of Steps	1	5	10	20	50	100
Nº of lines	10x10	50x50	100x100	200x200	500x500	10^3x10^3
Data points	100	$2.5\ 10^3$	10^4	$4\ 10^4$	$2.5\ 10^5$	10^6
Inform(Kb)	1.6	40	160	640	$4\ 10^3$	$16\ 10^3$
Time (s)	10	120	10^3	$2\ 10^4$	$2\ 10^5$	$3\ 10^6$

The exponential increase in the amount of information obviously stems from the fact that each of the intersections of lines at every recording yields a valid data point value. If the number of bright lines in the shadow pattern were larger, the amount of information would be impractical.

It must also be taken into account that in cases where the bright lines in the shadow patterns are very close to each other, it is hard to discern whether the line considered belongs to one register or another. Lines are not vertical or horizontal, as they deviate from the ideal shape following the wavefront aberrations, and too many lines will complicate assigning its correct position value to them.

Our experience is that microstepping procedures yielding around 10^4 measured values are the most suitable. This means ten steps in one period of a ronchigram with ten lines in the Ronchi pattern, which means that around 100 vertical and horizontal lines will be considered valid, and that about 400 of the vertical and horizontal remaining pixels will be considered not to contain any data value. This 1 to 4 ratio accounts for a reasonable separation between consecutive lines. Furthermore, the integration time remains acceptable (some minutes). However, some measurements were carried out with ten steps in a ronchigram with 20 bright lines, yielding $4\ 10^4$ data

points. Although the results yielded the right values for the radius of curvature, the surface reconstruction time took some hours.

So, to summarize Section 5.3, microstepping has provided us with a tool that provides a substantial increase in our ability to measure surfaces through the Ronchi test technique. Obtaining an additional set of measured data values through lateral displacements of the Ronchi test allows us to improve the sampling of the surface as we wished, without increasing the amount of diffractive effects present in the observation plane. This kind of process is easily applied to the experimental setup presented in Section 4.